Calibration of Historical and Future AVHRR and GOES Visible and Near-Infrared Sensors and the Development of a Consistent Long-Term Cloud and Clear-Sky Radiation Property Dataset

Bi-annual Project Report
6/01/2010 – 11/30/2010
Award: NA10AANEG0158

Principal Investigator: Patrick Minnis (p.minnis@nasa.gov)
NASA Langley Research Center, Hampton, VA

Co-Investigators: David R. Doelling, Louis Nguyen
NASA Langley Research Center, Hampton, VA

Xiangqin Wu
NOAA NESDIS, Silver Spring, MD

Xiaxiong Xiong
NASA Goddard Space Flight Center

CDRs Addressed

Multispectral Imager(s) Solar Reflective (SDR)
Cloud Properties (Amount, Height, Phase, Optical Depth, Effective Particle Size) TCDR
Clear-Sky Radiance TCDR

1. Introduction

A stable and consistent set of imager radiances is an essential component of any long-term satellite climate data record (CDR). Calibrated imager radiances are critical for retrieving climate quality geophysical parameters needed for monitoring climate. Two sets of those parameters, cloud properties and the properties of the complementary clear scenes, are important components of the climate system since they affect the radiation balance and hydrological cycle. While several different groups around the world are involved in calibrating imagers on polar orbiters such as the Advanced Very-high Resolution Radiometer (AVHRR) series, and on geostationary satellites (GEOsat) imager, there are many different methods for effecting those calibrations. Similarly, cloud and surface climatologies are being or have been developed by different groups around the globe, but the satellite imager data are being analyzed in different ways resulting in differences among the results. It is this variety of methods and results that helps establish the uncertainties in the resulting calibrations and geophysical parameters allowing an assessment of the confidence in their climatological variations. This project focuses on two goals, imager solar channel calibration to develop a coherent reflected radiance Fundamental CDR (FCDR) and cloud and clear-sky property retrievals to provide a Thematic CDR (TCDR) of cloud and clear parameters consistent with their counterparts determined for the Clouds and Earth's Radiant Energy System (CERES). CERES is a climate project charged with monitoring the Earth's radiation budget, the fundamental energy source driving weather and climate. This report summarizes the work accomplished during the first 6 months of this effort.

1.1 Calibration FCDR

The calibration FCDR is focused on is the development of a coherent reflected radiance Fundamental CDR (FCDR) for the AVHRR and geostationary satellite (GEOsat) imagers extending back to 1978. To accomplish this goal, we are applying mature and robust calibration algorithms, specifically, the Nearly Simultaneous Ray-matched Technique (NSRT), stable desert target method (SDTM), and the Deep Convective Cloud Technique (DCCT). These methods were used to uncover errors in the MODIS and TRMM VIRS records for visible and infrared calibrations. We are developing a semi-automated method for applying the methods and applying them in real time with quality control constraints. Uncertainties will be developed from comparisons of results from the three methods.

1.2 Cloud and clear TCDR

The cloud TCDR consists of cloud amount, phase, optical depth (COD), effective particle size, height, and temperature. The clear TCDR will consist of clear-sky albedos and clear-sky surface skin effective temperatures. These TCDR parameters are being developed in a manner that is as consistent as possible with that used to retrieve the CERES cloud properties from the MODerate-resolution Imaging Spectroradiometer (MODIS). To date, the CERES cloud properties have been derived using MODIS data since 2000 and will continue to be retrieved using data from the Visible Infrared Imager Radiometer Suite (VIIRS) on future low Earth-orbiting satellites (LEOsats). Because the CERES Edition-4 analysis uses more than seven of the MODIS channels (Minnis et al., 2010a), modifications are being made to the algorithms for application to the 5-channel AVHRR data. The results of this analysis should be extremely valuable for climate studies. We will be collaborating with other CDR teams to ensure non-redundancy and optimization of the products.

2. Accomplishments to date and to be completed by end of period

The tasks scheduled for the first year of this study are summarized in Table 1. Progress on each task and plans for the next 6 months are outlined below.

2.1 Set up quality control standards for the NSRT and DCCT

The solar channels are being calibrated against the MODIS imagers because they have extremely stable gains as a result of having onboard calibration systems lacking on all of the operational satellite imagers. Both the NSRT and DCCT are being used to effect transfers of the MODIS calibration back in time. The NSRT is being used to transfer the MODIS calibrations to contemporaneous AVHRR and GEOSat instruments. Those calibrations will be transferred to older satellite imagers in the same manner using overlapping time periods. The DCCT serves as an independent method to compute trends in the calibration coefficients. This will be checked against the SDRM results and compared with results from other groups (ISCCP and NOAA CIMSS). Spectral differences between channels will be taken into account using the spectral filter functions and SCHIAMACHY high-spectral resolution measurements.

2.1.1 NSRT

For a given solar reflectance channel *i*, the effective radiance measured by the sensor is

$$L_i = \int_{\lambda_{1i}}^{\lambda_{2i}} F_{\lambda i} L_\lambda d\lambda, \qquad (1)$$

where $F_{\lambda i}$ is the band spectral response function (SRF), λ is the wavelength, and λ_{1i} and λ_{2i} are wavelength limits of the band. The sensor measurement is given in counts C and usually assumed to be linear in radiance.

$$L_i = g_i\,(C - C_o), \qquad (2)$$

where g is the sensor gain and C_o is the offset or space count. The reflectance is

$$\rho_i = L_i / \mu_o E_i, \qquad (3)$$

where the band solar constant is

Table 1. Scheduled tasks for 1 June 2010 – 31 May 2011.

Year 1	• Set up QC standards for NSRT & DCCT • Complete automated integration software for DCCT & NSRT calibrations • Process contemporaneous AVHRR calibrations (N15, 16, 17, 18) • Evaluate MODIS data to establish references and uncertainties • Perform desert site calibrations • Calibrate contemporaneous GEOsat calibrations (2000-present) • Set up global automated cloud analysis system to apply to AVHRR • Perform error analyses for 4 and 5-channel cloud retrievals w/ sampled MODIS data • Refine polar retrieval method to incorporate improved snow albedo and SIST • Analyze contemporaneous AVHRR data (N16, 17, 18) • Compute SRF ratios from SCHIAMCHY data

$$E_i = \int_{\lambda_{1i}}^{\lambda_{2i}} F_{\lambda i} E_{\lambda o} d\lambda, \quad (4)$$

where $E_{\lambda o}$ is the Earth-sun distance corrected spectral solar constant radiance and μ_o is the cosine of the solar zenith angle SZA.

Because simultaneous nadir observations between two satellites is a relatively rare event, the NSRT is used to increase the sampling and dynamic range for a given pair of satellites. To match a given pair of satellites, the data from each imager are averaged on a 0.25° grid. Only those collocated data that are taken within ±15 min of other are used. No data are used that are potentially affected by significant sunglint, large anisotropy, or when the difference between the respective viewing zenith angles VZA or relative azimuth angle RAA from the two satellites is less than 10° or 15°, respectively. Except for some DCC systems, all data are taken over ocean. For two satellites, A and B, it is assumed that the reflectances for a given scene should be the same, therefore, the radiance for target satellite A is normalized to the solar constant and SZA of reference satellite B. Thus, for a given pair of measurements,

$$L_B = \frac{\mu_{oB} E_B}{\mu_{oA} E_A} L_A. \quad (5)$$

Similarly, L_b can be related to the counts for satellite A. One month of matched data is used in a linear regression to obtain the gain g_A for satellite A for the month. All gains over a given time period are then fit to a line or polynomial to determine the trends in the calibration. The fits typically take the form,

$$g(\mathrm{DSL}) = g_o + a_1\, DSL + a_2\, DSL^2, \quad (6)$$

where DSL is the number of days since launch of the satellite.

This method can be applied from LEOs to LEOs, LEOs to GEOsats, vice versa, and GEOsats to GEOsats. For the latter method, the approach of Minnis (1989) is employed. Only data taken near local noon at the longitude centered between the two GEOsat subsatellite points are used in the regressions. The NSRT yields absolute gains in physical units.

2.1.2 DCCT

The DCCT assumes that, over time, the albedo of DCC's is invariant, statistically speaking. Probability distribution functions (PDF) of normalized VIS (0.64 μm) radiances are constructed each month over ocean for all pixels i between 30°N and 30°S that meet all of the following criteria:

$$T_{11i} < 205.0\ \mathrm{K},\ SZA < 40°,\ VZA < 40°,\ 10° < RAA < 170°,\ \sigma(T_{11}) < 1.0\ \mathrm{K},\ \text{and}\ \sigma(\rho) < 0.02\ \rho_i,$$

where T_{11} is the IR channel brightness temperature, and σ is the standard deviation of the specified quantity for the subject pixel and its eight adjacent pixels. The value of L_i is first corrected for anisotropy to obtain a Lambertian-equivalent radiance L_{Ni} by multiplying by the appropriate theoretical DCC anisotropic correction factor (ACF). The resulting spectral radiance is then normalized to SZA = 0° using an SZA-dependent albedo model (SAM). The normalized radiances taken during the month are then used to form a PDF and compute the mean and mode

radiances. The trends in the modes and means are determined from time series of each quantity by normalizing to the values for a selected month, either the center or beginning of the time series. As the sensor degrades the mean and mode counts decrease, so the gain must increase. The actual gain then is

$$g(\mathrm{DSL}) = G(\mathrm{DSL}) * g(\mathrm{REF}) / G(\mathrm{REF}), \tag{7}$$

where G is the normalized gain and REF indicates the DSL when an absolute calibration value is available. Equation (7) transfers the absolute calibration to any day, DSL, by taking out the trend.

2.1.3 Quality control

The quality of the NSRT and DCCT calibrations depends on a variety of factors including number of samples, dynamic range, SZA, viewing angles, and location. To develop QC constraints, the processing has been performed using essentially no constraints, other than those specified above, to determine the types of conditions leading to instability or large scatter in the results. For example, the available ACFs become less certain with increasing SZA, so the DCCT may not be useful for a range of large SZAs until better ACF and SAM are available. By segregating the data by region, we have found differences between the typical DCC albedos over the tropical western Pacific and the rest of the globe that appear to be due to differences in particle size near cloud top. For the DCCT, we have been exploring the use of the skewness and kurtosis of the PDFs as possible means of removing errant data. In the coming months, we will be exploring that approach and others to minimize the noise in the gains.

2.2 Complete automated integration software for DCCT and NSRT calibrations

Prior to integrating the DCCT and NSRT calibrations in order to apply (7), the component software must first be established and in good working order. The NSRT and DCCT algorithms have been finalized and a system for automatically integrating them is under development. An internal display system has been developed for easy viewing and assessment of the results. This display system will serve as the prototype for a web page that will provide the calibration coefficients to the public. During the second half of the year, we will continue working on this software system to facilitate processing of the intercalibrations of each satellite.

2.3 Process contemporaneous AVHRR calibrations for NOAA 15, 16, 17, and 18

Because of priorities in processing, we have decided to concentrate on the afternoon NOAA (N) satellites first and then process the morning orbiters. To date, we have performed the initial DCCT and NSRT calibrations for N14, N16, and N18. The DCCT normalized gains in the channel 1 visible (VIS; 0.65 µm) and channel-2 near-infrared vegetation (VEG; 0.86 µm) calibrations are shown in Figs. 1 and 2 for N18 and N14, respectively. The gains for both channels vary nonlinearly, changing by ~0.03 and ~0.045 for channels 1 and 2, respectively, during the first year and then taking another 2-3 years to change the same amount after mid 2006.

The longer record of N14 (Fig. 2) reveals a steeper degradation of gains for both channels, but the 0.86-µm gain levels off with, perhaps, a slight downward trend after 1997. The 0.65-µm gain continues increasing into 1999 before dropping. The scatter in G increases for both channels after the start of 2000. By that time, N14 had drifted into a near-terminator orbit resulting in

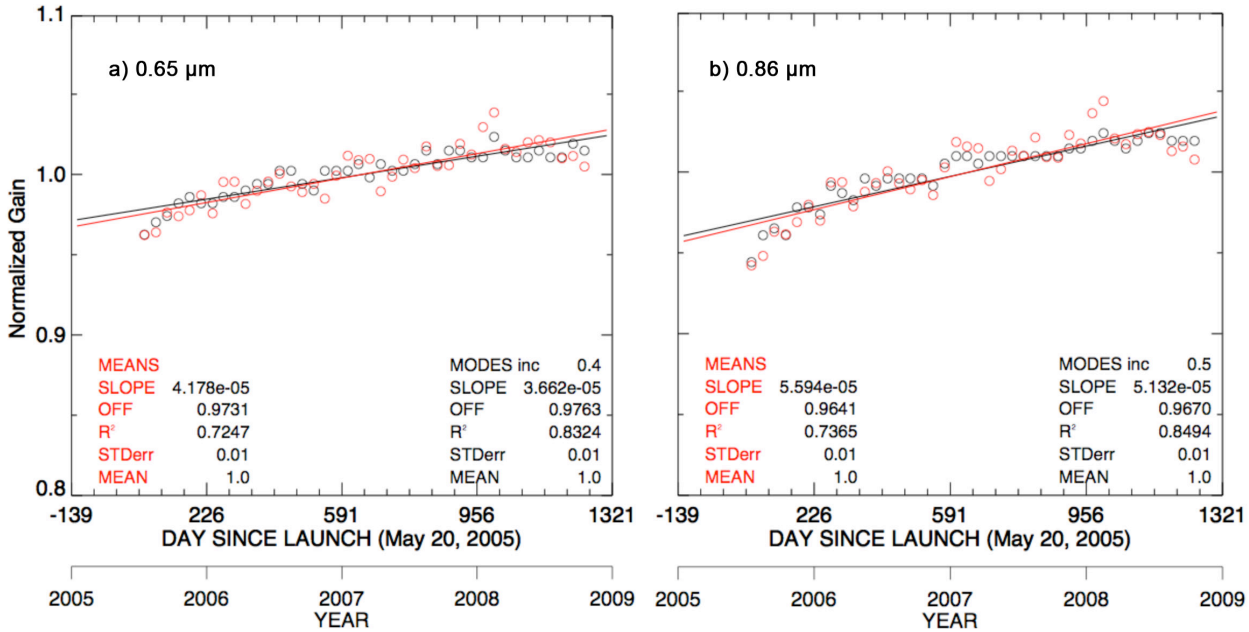

Fig. 1. Normalized gains in N18 AVHRR channels (a) 1 and (b) 2 from DCCT for 2005 - 2008.

much reduced dynamic range because of the large SZAs. This apparent SZA dependence will be investigated further to establish QC constraints as noted above.

Because we are tasked with cross-calibrating the GEOSat imagers and normalizing them to MODIS and the matching of the GEOSats and LEOSats is relatively straightforward, we have performed our initial calibrations of the AVHRRs by first intercalibrating the MODIS and GEOSats, then calibrating the AVHRR data using the GEOSats. In this initial effort, we did not not apply the SRFs. That step will be taken in the final calibrations after development of the methods for using the SRFs is completed (see section 2.9).

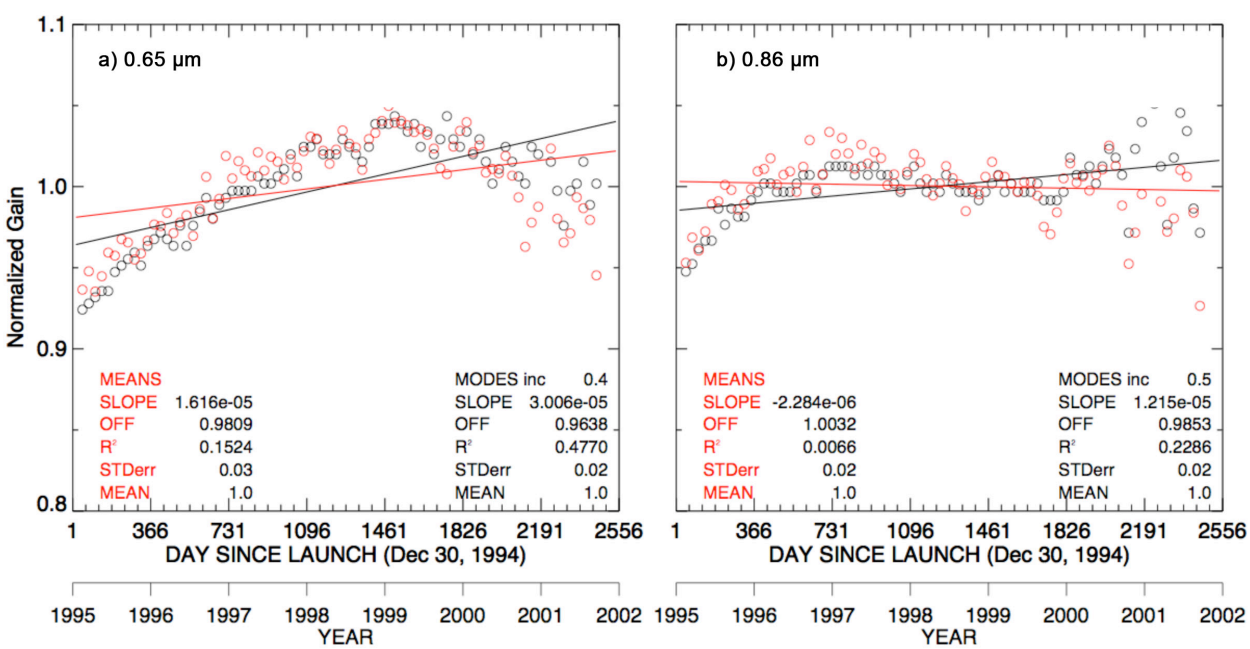

Fig. 2. Normalized gains in N14 AVHRR channels (a) 1 and (b) 2 from DCCT for 2005 - 2008.

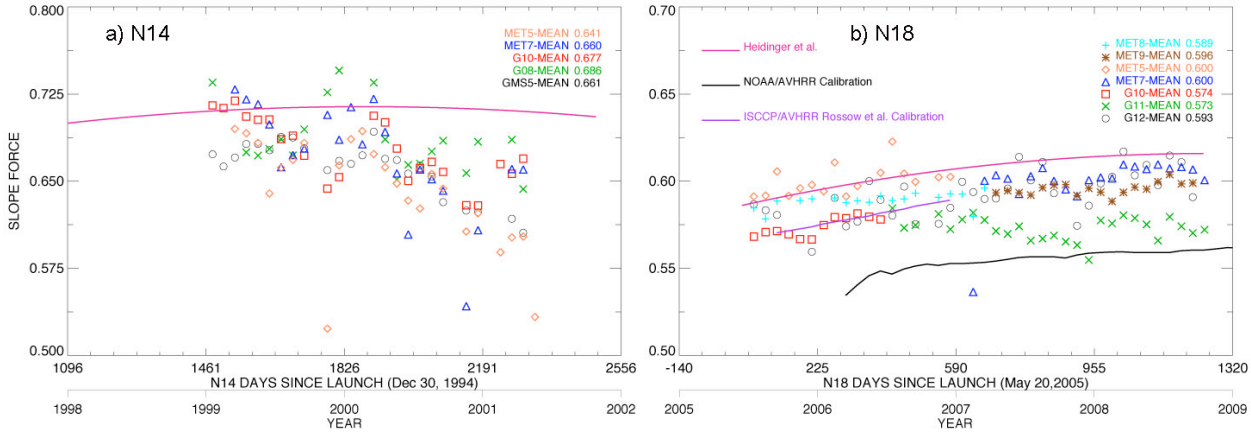

Fig. 3. Trends in AVHRR channel-1 gain determined from intercalibrations with MODIS-calibrated GEOSat imager VIS channels using force fits through "known" space counts.

The VIS channels of the various GEOSat imagers were intercalibrated against Terra MODIS using the NSRT and, when necessary, their gains were projected back in time before the launch of Terra using polynomial fits to the monthly gains derived over the period when both AVHRR and MODIS data were available. The NSRT was then used to calibrate the AVHRR channels against the different GEOSat imagers. Figure 3 shows the gains derived using this technique for N14 (Fig. 3a) and N18 (Fig. 3b) several Meteosat (MET) and Geostationary Operational Environmental Satellite (GOES) imagers as well as the Geostationary Meteorological Satellite (GMS). The curves corresponding to other calibration sources are also shown. The calibrations from Heidinger et al. (2010) are shown in both plots, while the calibrations from the International Satellite Cloud Climatology Project (ISCCP; Rossow and Schiffer et al., 1999) and NOAA are shown for N18 (Fig. 3b). No NSF corrections have been applied to any of the calibrations. The curves from Heidinger et al. (2010) correspond to the highest values from the GEOSat intercalibrations. For N18, the highest values of *g* are mostly from MET5, MET7, and GOES12 (G12) while the lowest values are from G10 and G11. The generally greater values from Heidinger et al. (2010) may be due to their use of both Terra and Aqua to establish their fits. Minnis et al. (2008) demonstrated that the Terra MODIS VIS channel radiances are 1% less their Aqua counterparts before November 2003, and ~2.1% lower after that time period. The 1.1% change after 2003 has been taken into account in Fig. 3, but not the original 1% difference. The ISCCP gains are ~3% less than the Heidinger values and ~6% greater than the NOAA values. Except for the G11 results, the N18 GEOSat gains are generally between the two datasets. We expect that applying the NSF corrections will tighten up the scatter among the different GEOSat-based gains.

For N14, the seasonal variations in the GEOSat gains appear to have significant seasonal variations. Again, the Heidinger curve is closest to the highest values determined from the GEOSat data. Most of the GEOSat-retrieved gains drop off rapidly after the beginning of 2000, similar to the changes seen from the DCCT values of *G* in Fig. 2a. The scatter in *g* also increases after 1999. Here, the increase in SZA results in smaller dynamic ranges causing an increase in the uncertainty of the fit.

During the rest of Year 1, we will

- perform direct cross-calibrations between MODIS and AVHRR for post1999 period.
- apply NSF corrections to both AVHRR and GEOSat imagers
- examine the consistency between the DCCT and NSRT results

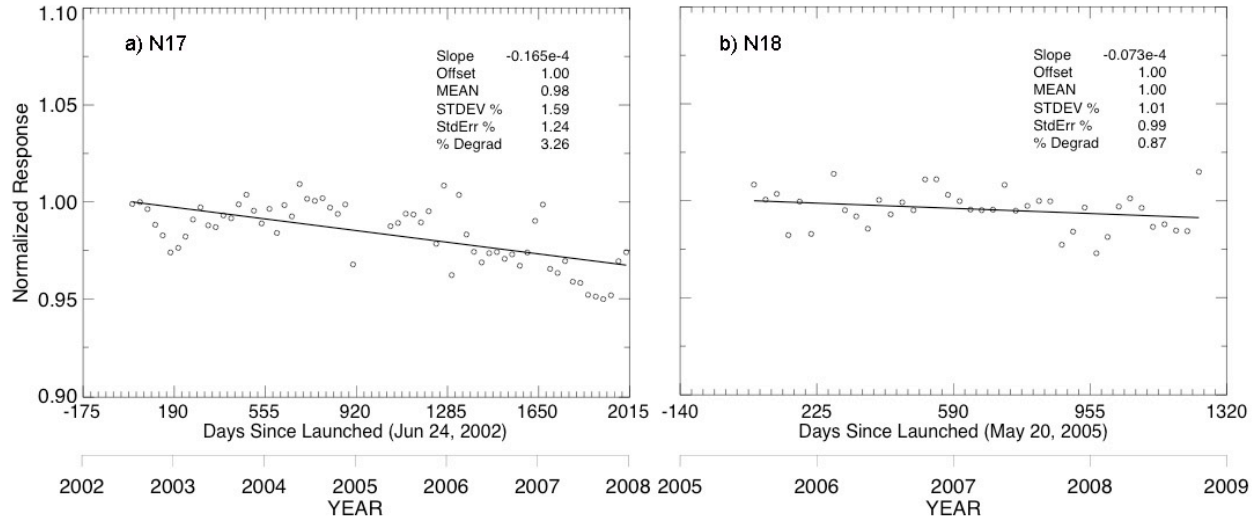

Fig. 4. Trends in normalized AVHRR channel-1 gain determined from measuring the average albedo over the clear Libyan desert.

- normalize Terra MODIS to Aqua MODIS to eliminate MODIS artifacts
- determine the errors in g resulting from use of GEOSats to provide the absolute calibration of the DCCT results in the pre-MODIS time frame.

2.4 Perform desert site calibrations using DSRT

The desert sites provide an independent measure of the calibration trends. We have just begun the process of performing desert monitoring of the trends in the AVHRR gains. The DSRT assumes that the selected desert site albedos are temporally invariant and stable because of their lack of vegetation and rainfall. Beginning with an initial gain g_o, the albedo of the scene is

$$\alpha_o(\mathrm{SZA}_o) = \rho_o / \chi(SZA_o, VZA, RAA), \qquad (8)$$

where χ is the bidirectional reflectance distribution function (BRDF). By measuring reflectance at the same SZA and having the BRDF, the trend can be determined by continuously monitoring the site. Because the NOAA satellites often drift in orbit and the overpass SZA changes seasonally and cyclically, it is also necessary to account for the variation of albedo with SZA. This done using a normalized directional reflectance model δ(SZA), defined as the ratio of the albedo at a given SZA to that at SZA = 0°. Thus, the albedo at some time, DSL, can be normalized to the initial value and a normalized gain can be computed as follows.

$$G(\mathrm{DSL}) = \alpha(\mathrm{DSL}, \mathrm{SZA}) * \delta(\mathrm{SZA}_o) / \alpha_o(\mathrm{SZA}_o) / \delta(\mathrm{SZA}). \qquad (9)$$

This process was performed over the Libyan desert site for N17 and N18. The results are shown in Fig. 4. The linear fits indicate that the N17 VIS channel is degrading at more than twice the rate of that for N18. The scatter in the data suggests that there are some possible seasonal variations in α_o and some events that actually change the surface albedo.

In Fig. 4b, the N18 shows a gain degradation of only 1% in 3.5 years. The other methods suggest greater changes in the gain for that same period. The DCCT (Fig. 1a) change is ~5% and

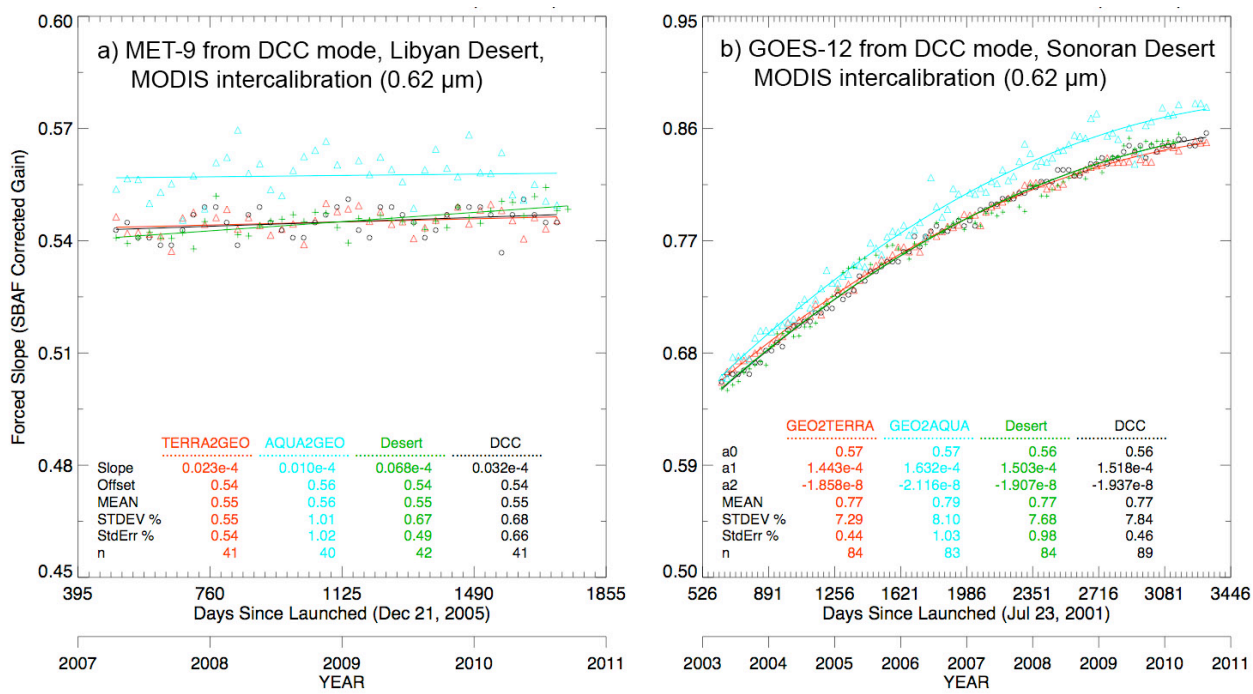

Fig. 5. Trends in linear gains for VIS channels on (a) MET-9 and (b) GOES-12 using 3 techniques and two reference sensors (MODIS on Aqua and Terra). Normalized curves for desert and DCC calibrated using Terra MODIS at mid points of curves.

the NSRT change is ~3% for the MET-8/MET-9 comparisons in Fig. 3b. These inconsistencies are precisely why we are performing the calibrations using several different methods.

In the next 6 months, we will be examining these datasets to determine how much of the differences can be reconciled. For example, a non-linear fit to the DCCT data will reduce the trend, while a direct comparison with MODIS will likely yield a different result than a transfer from MODIS to AVHRR using Meteosat. The relatively large noise seen in Fig. 4 may also play a role in the retrieved slopes.

2.5 Calibrate contemporaneous GEOsat calibrations (2000-present)

We have set up a system to calibrate the GEOsats against MODIS and AVHRR (e.g., Fig. 3). The MTSAT visible sensor is particularly difficult, but we have developed a method to deal with its behavior at the low end of its dynamic range (Doelling et al., 2010b). Figure 5 shows the entire suite of methods applied to the MET-9 (Fig. 5a) and GOES-12 (Fig. 5b) VIS channels (Morstad et al. 2010). These gains have been corrected using the SRF correction curves based on SCHIAMACHY data (Doelling et al. 2010a; Scarino et al. 2010). The MET-9 and GOES-12 gains based on Aqua MODIS are 2-3% and 0.5 – 3.5% greater than their Terra counterparts due to the inherent differences between the two MODIS sensors and the changing Terra MODIS gains with time (Minnis et al., 2008). Since the Aqua MODIS is the more stable of the two instruments, it will be used as the calibration standard. Unlike the AVHRR plots, the DCC and desert calibrations are in remarkably good agreement with the direct calibrations using the Terra MODIS. During the coming months, we will continue the intercalibrations working back to 2000 while monitoring the current satellite imager calibrations.

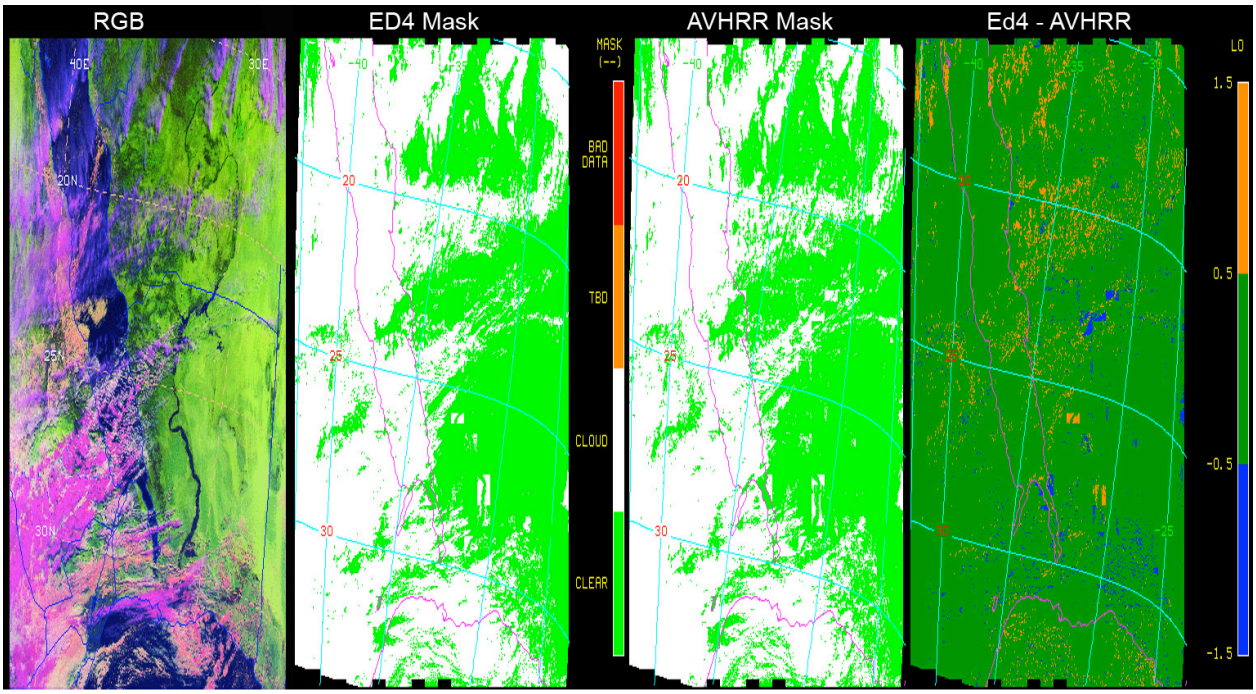

Fig. 6. Example of cloud masks applied to Aqua MODIS data using CERES Ed4 algorithm (center left) and AVHRR 5-channel algorithm (center right) for 08 UTC, 31 July 2008 over Red Sea. Difference between Ed4 and AVHRR mask (right) shows AVHRR missed (added to) Ed4 clouds in orange (blue). North is toward bottom of images.

2.5 Set up global automated cloud analysis system to apply to AVHRR

The automated analysis system has been set up to read in all of the appropriate inputs and the initial algorithms have been implemented for testing. During the remainder of the year, the algorithms will be refined to match the CERES Ed4 analyses as closely as possible.

2.6 Perform error analyses for 4 and 5-channel cloud retrievals w/ sampled MODIS data

Our initial comparisons of the CERES Ed4 and AVHRR mask have begun. Figure 6 shows an example of the results for an area centered on the Red Sea. The masks are generally quite close with the AVHRR mask missing clouds along the edges of high clouds detected by Ed4 (orange) and adding some clouds over some of the northernmost land areas and the edges of water features. During the remainder of the year, we will further refine the mask to better match the Ed4 retrievals before applying it to the AVHRR datasets.

2.7 Refine polar retrieval method to incorporate improved snow albedo and SIST

We have begun working on improved detection and retrieval of clouds over snow using the AVHRR channels by first developing improved albedo maps for the VIS and VEG channels. At the same time, we have been working on a multi-tiered approach to use different channels depending on the apparent optical depth. The SIST (Shortwave Infrared Split-window Technique) uses the 3.7, 11, and 12 µm channels at night and is useful only for optically thin clouds. We are researching the thresholds needed to invoke its use during the day over snow so that we do not overestimate the COD for thin clouds (Bedka et al. 2010; Heck et al., 2010). We are also looking at the use of the VIS and VEG channels together to improve the COD retrieval for thicker clouds. We are using the Ed4 retrieval using the 1.24-µm channel (Minnis et al.,

2010b; Palikonda et al., 2010) along with the 2.1-µm channel retrievals as the truth for retrieving the cloud optical depth over snow.

During the next 6 months, we will complete 1-year of snow albedo map production and have our initial thin-thick thresholds determined for testing. The initial testing of the two-channel COD retrieval will be completed.

2.8 Analyze contemporaneous AVHRR data (N16, 17, 18)

These analyses have not begun because the algorithms are still being refined (see above). For the remainder of this year, we will begin our analyses with N18 AVHRR data, but simultaneously analyze the N9 AVHRR data to facilitate the ERBE analyses of the S. Kato research.

2.9 Compute SRF ratios from SCHIAMCHY data

We demonstrated the utility of the SCHIAMACHY data for removing the SRF differences between the various imager channels by performing intercalibrations separately over land and ocean using MODIS and GOES-12 data and filter functions. The SRF corrections based on SCHIAMACHY data reduced the differences between the gains computed over land and ocean from 10% to less than 1% (Doelling et al. (2010a). These corrections were then developed for all of the current GEOsats (Scarino et al., 2010) and then applied to the GEOsat-MODIS intercalibrations (e.g., Fig. 5). During the rest of the year, we will develop the corrections for the AVHRR channels.

References

Heidinger, A. K., W. C. Straka III, C. C. Molling, J. T. Sullivan, and X. Wu, 2010: Deriving an inter-sensor consistent calibration for the AVHRR solar reflectance data record. *Intl. J. Remote Sens.*, 31, 6493-6517.

Minnis, P., 1989: Viewing zenith angle dependence of cloudiness determined from coincident GOES East and GOES West data. *J. Geophys. Res.*, **94**, 2303-2320.

Minnis, P., D. R. Doelling, L. Nguyen, W. F. Miller, and V. Chakrapani, 2008: Assessment of the visible channel calibrations of the TRMM VIRS and MODIS on *Aqua* and *Terra*. *J. Atmos. Oceanic Technol.*, **25**, 385-400.

Minnis, P., S. Sun-Mack, Q. Z. Trepte, F.-L. Chang, P. W. Heck, Y. Chen, Y. Yi, R. F. Arduini, K. Ayers, K. Bedka, S. Bedka, R. Brown, S. Gibson, E. Heckert, G. Hong, Z. Jin, R. Palikonda, R. Smith, W. L. Smith, Jr., D. A. Spangenberg, P. Yang, C. R. Yost, and Y. Xie, 2010a: CERES Edition 3 cloud retrievals. *AMS 13th Conf. Atmos. Rad.*, Portland, OR, June 27 – July 2, 5.4.

Rossow, W. B. and R. A. Schiffer, 1999, Advances in understanding clouds from ISCCP. *Bull. Amer. Meteorol. Soc.*, **80**, 2261-2287.

Sun-Mack, S., P. Minnis, Y. Chen, S. Kato, and D. Winker, 2010: Cloud property comparisons among CERES, CALIPSO Version 2, and CALIPSO Version 3. *Earth Radiation Budget Workshop 2010*, Paris, France, Sept. 13-16.

Publications and presentations to date (some also referenced)

Doelling, D. R., C. Lukashin, P. Minnis, B. Scarino, and D. Morstad, 2010a: Spectral reflectance corrections for satellite intercalibrations using SCIAMACHY data. Submitted to *Geosci. Remote Sens. Lett.*

Goldberg, M., G. Ohring, J. Butler, C. Cao, R. Datla, D. Doelling, V. Gärtner, T. Hewison, B. Iacovazzi, D. Kim, T. Kurino, J. Lafeuille, P. Minnis, D. Renaut, J. Schmetz, D. Tobin, L. Wang, F. Weng, X. Wu, F. Yu, P. Zhang, and T. Zhu, 2010: The Global Space-based Inter-Calibration System (GSICS), *Bull. Am. Meteorol. Soc.*, in press.

Bedka, S., P. Minnis, P. W. Heck, D. P. Duda, R. Palikonda, K. Khlopenkov, and R. Boeke, 2010: Retrievals of daytime and nighttime cloud macro- and microphysical properties using infrared satellite observations. *AMS 17th Conf. Satellite Meteorology & Oceanography*, Annapolis, MD, Sept. 27-30, P1.9.

Doelling, D. R., R. Bhatt, D. Morstad, and A. Gopalan, 2010b: The calibration of geostationary visible sensors using MODIS as a reference for GSICS. *CALCON 2010 Tech. Conf.*, Logan, UT, August 23-26.

Heck, P. W., P. Minnis, S. T. Bedka, R. Palikonda, Y. Yi, M. M. Khaiyer, and F.-L. Chang, 2010: Cloud property retrievals from satellite data using thermal wavelengths in daytime and nighttime. *AMS 13th Conf. Atmos. Rad. and Cloud Phys.*, Portland, OR, June 27 – July 2, JP1.25.

Minnis, P. W. L. Smith, Jr., S. Sun-Mack, Y. Chen, D. A. Spangenberg, R. Palikonda, and R. F. Arduini, 2010b: Retrieving cloud properties over snow and ice surfaces. *3rd Intl. Symp. Recent Advances in Quantitative Remote Sens.*, Valencia, Spain, September 27-October 1, S3.1.

Morstad, D., D. R. Doeliing, B. Scarino, A. Gopalan, R. Bhatt, and P. Minnis, 2010: AVHRR calibration approach that uses ray-matching, invariant desert, and deep convective cloud techniques. *2010 AGU Fall Mtg.*, San Francisco, CA, December 13-17, A13G-0304.

Palikonda, R., P. Minnis, M. L. Nordeen, D. A. Spangenberg, B. Shan, P. W. Heck, Q. Z. Trepte, and T. Chee, 2010: Improvements to cloud detection and optical properties over snow background from geostationary satellite data. *AMS 13th Conf. Atmos. Rad. and Cloud Phys.*, Portland, OR, June 27 – July 2, JP1.34.

Scarino, B., D. R. Doelling, D. Morstad, A. Gopalan, P. Minnis, R. Bhatt, and C. Luckachin, 2010: Absolute calibration of AVHRR visible sensors using SCIAMACHY hyperspectral data and MODIS radiances. *2010 AGU Fall Mtg.*, San Francisco, CA, December 13-17, A13G-0303.